R. & M. No. 3295

MINISTRY OF AVIATION

AERONAUTICAL RESEARCH COUNCIL
REPORTS AND MEMORANDA

The Leading-Edge Buckling of a Thin Built-up Wing due to Aerodynamic Heating

By K. I. McKenzie, Ph.D.

LONDON: HER MAJESTY'S STATIONERY OFFICE
1962
TEN SHILLINGS NET

The Leading-Edge Buckling of a Thin Built-up Wing due to Aerodynamic Heating

By K. I. McKenzie, Ph.D.

Communicated by the Deputy Controller Aircraft (Research and Development), Ministry of Aviation

Reports and Memoranda No. 3295 *

February, 1961

Summary. An analysis is presented of the buckling of the leading edge of a thin built-up wing subjected to spanwise thermal stress. Computed values of the buckling load are given in graphical form for a wide variation of leading-edge dimensions and these results are used to obtain buckling criteria for some specific examples.

1. *Introduction.* When a wing is subjected to aerodynamic heating, the leading edge becomes hotter than the central portion partly because it has less thermal capacity, and partly because the aerodynamic heat-transfer coefficient is larger there than elsewhere in the wing[1]. Thus there is a spanwise compressive thermal stress in the region near the leading edge which may cause buckling.

The leading-edge buckling of a solid wing or a wing with a continuous shear filling has been treated by Mansfield[2]. In this paper the same problem is considered for a built-up wing. The leading-edge construction considered consists of two skins effectively built-in to a spar along one edge, with their other edges rigidly attached to a fillet of triangular cross-section. The mechanisms by which the leading edge may be stressed in practice are various, depending on the heating conditions and the design of the whole wing, but conditions can be envisaged where the compressive stress in the fillet was either higher or lower than that in the skin, and even where the fillet was in tension while the skin was in compression. The spanwise stress in the skin is taken to be constant across the width and that in the fillet an arbitrary multiple of that stress. If there is no stress in the fillet the buckling stress for such a structure varies between that for a long plate built-in along one edge and free along the other and that for a plate built-in along both edges. However, if there is a compressive stress in the fillet the structure may buckle at a value of the stress in the skin even lower than that for the clamped-free plate.

The effect on the buckling load of chordwise ribs is estimated by calculating the variation of buckling stress with wavelength in some particular examples. It is found that in most cases the ribs have only a small effect provided the distance between them is more than three times the distance between the fillet and the first spar. However, when the effective end load on the fillet is high compared to the stress in the skin, the spanwise waves become long and ribs can provide a considerable stabilising effect.

The critical temperatures and stresses for five examples of possible leading-edge designs are given.

* Previously issued as R.A.E. Report No. Structures 259—A.R.C. 22,982.

2. *Assumptions.* The usual assumptions of small-deflection theory are made together with the following:

(1) The spanwise compressive stress is constant across the width of skin between fillet and first spar; and the stress in the fillet is an arbitrary multiple of that constant.

(2) The angle 2θ between the two skins at the leading edge is such that $\cos\theta \doteqdot 1$.

(3) The skin is rigidly built-in both to the first spar and to the fillet. The spar is perfectly rigid and the fillet cross-section undeformable. The fillet has finite torsional and flexural rigidities consistent with its thin triangular cross-section. The torsional rigidity is calculated using St. Venant theory, no account being taken of the change in effective rigidity due to the type of loading, though an estimate of the magnitude of this effect may be obtained from Appendix II.

3. *The Derivation of the Condition for Buckling.* When the leading edge of a wing buckles under compressive spanwise stress, the initial buckled form may be represented by a function of the type

$$W = f(X)\sin\frac{\pi Y}{l}, \tag{1}$$

where X is the chordwise and Y the spanwise co-ordinate and W the deflection perpendicular to the mid-chord. If the wing cross-section is symmetrical about the mid-chord, the deflection of the leading edge itself will be perpendicular to the mid-chord. In the present case the wing consists of two skins stiffened by spanwise members, the design of the leading edge being that shown in Fig. 1a. Thus, provided assumption (3) of the previous section holds, each skin will undergo a displacement in its own plane at the junction with the fillet given by

$$u = \tan\theta\left(w + b\frac{\partial w}{\partial x}\right)_{\text{evaluated at junction}} \tag{2}$$

where x is the co-ordinate shown in Fig. 1c and w is the deflection in the positive z-direction. This displacement will give rise to a system of plane stress in the skin which in turn will affect the boundary conditions at the junction between skin and fillet. However, this system of plane stress does not alter the differential equation governing the bending of the skin because terms arising from it are of the second order of smallness. The relevant differential equation therefore is that given by Timoshenko[3], namely

$$D\nabla^4 w = -N_y\frac{\partial^2 w}{\partial y^2}, \tag{3}$$

with conditions for a clamped edge applied at $x = 0$ and conditions necessary for the equilibrium of the fillet in bending and torsion at $x = a$.

Substituting the solution

$$w = f\left(\frac{x}{a}\right)\sin\frac{m\pi y}{a} \tag{4}$$

into equation (3) and writing

$$\psi^2 = \frac{N_y a^2}{D}, \tag{5}$$

the differential equation

$$f''''\left(\frac{x}{a}\right) - 2m^2\pi^2 f''\left(\frac{x}{a}\right) + m^2\pi^2(m^2\pi^2 - \psi^2)f\left(\frac{x}{a}\right) = 0 \tag{6}$$

is obtained. The general solution of this equation can be written

$$f\left(\frac{x}{a}\right) = C_1 e^{-\alpha x/a} + C_2 e^{\alpha x/a} + C_3 \sin\frac{\beta x}{a} + C_4 \cos\frac{\beta x}{a} \tag{7}$$

where

and

$$\left.\begin{aligned}\alpha^2 &= m\pi(\psi + m\pi)\\ \beta^2 &= m\pi(\psi - m\pi)\end{aligned}\right\}. \tag{8}$$

The conditions at $x = 0$ are those for a built-in edge, namely

$$f(0) = 0 = f'(0) \tag{9}$$

and applying these to equation (7) gives

$$f\left(\frac{x}{a}\right) = A\left(\cosh\frac{\alpha x}{a} - \cos\frac{\beta x}{a}\right) + B\left(\frac{\sinh\frac{\alpha x}{a}}{\alpha} - \frac{\sin\frac{\beta x}{a}}{\beta}\right). \tag{10}$$

The forces acting on the fillet due to the distribution of plane stress in the skin, are determined in Appendix I to be a direct force given by

$$F = \frac{4Gh\tan\theta}{a(1+\nu)}\left[\frac{1 + \left(\frac{3-\nu}{1+\nu}\right)\frac{\sinh 2m\pi}{2m\pi}}{\left(\frac{3-\nu}{1+\nu}\frac{\sinh m\pi}{m\pi}\right)^2 - 1}\right]\left[f(1) + \frac{b}{a}f'(1)\right]\sin\frac{m\pi y}{a} \tag{11}$$

and a spanwise shear force given by

$$S = 2Gh\tan\theta\,\frac{m\pi}{a}\left[\frac{\frac{(3-\nu)(1-\nu)}{(1+\nu)^2}\left(\frac{\sinh m\pi}{m\pi}\right)^2 - 1}{\left(\frac{3-\nu}{1+\nu}\frac{\sinh m\pi}{m\pi}\right)^2 - 1}\right]\left[f(1) + \frac{b}{a}f'(1)\right]\cos\frac{m\pi y}{a}. \tag{12}$$

The shear forces due to top and bottom skins combine to exert a moment M_T on the fillet, where

$$M_T = 2c_1 S$$

and therefore there is an upward vertical force V_T on the fillet given by

$$V_T = -2c_1\frac{dS}{dy}. \tag{13}$$

Now the shear centre of the fillet is at its centroid (*see* Ref. 4), and therefore the deflection of the shear centre is given by

$$\left(w + \frac{b}{3}\frac{\partial w}{\partial x}\right)_{\text{evaluated at junction of skin and fillet.}}$$

Thus, using the notations shown in Fig. 1, the boundary condition for equilibrium of forces on the fillet is

$$2V_x\cos\theta + 2F\sin\theta + V_T + \frac{P}{\cos\theta}\left(\frac{\partial^2 w}{\partial y^2} + \frac{b}{3}\frac{\partial^3 w}{\partial x\partial y^2}\right)_{x=a} +$$

$$+ \frac{EI}{\cos\theta}\left(\frac{\partial^4 w}{\partial y^4} + \frac{b}{3}\frac{\partial^5 w}{\partial x\partial y^4}\right)_{x=a} = 0 \tag{14}$$

where P is the total end load on the fillet. The condition for equilibrium of moments is

$$2M_x + 2V_x \frac{b}{3}(1+2\sin^2\theta) - 2F\frac{2}{3}b\sin\theta\cos\theta + V_T\frac{1}{3}b\cos\theta + \\ + GJ\left(\frac{\partial^3 w}{\partial x \partial y^2}\right)_{x=a} = 0. \tag{15}$$

The expressions for M_x and V_x in terms of derivatives of the deflection are:

$$\left.\begin{aligned} M_x &= -D\left(\frac{\partial^2 w}{\partial x^2} + \nu\frac{\partial^2 w}{\partial y^2}\right)_{x=a} = -\frac{D}{a^2}\{f''(1) - \nu(m\pi)^2 f(1)\}\sin\frac{m\pi y}{a} \\ V_x &= -D\left(\frac{\partial^3 w}{\partial x^3} + (2-\nu)\frac{\partial^3 w}{\partial x \partial y^2}\right)_{x=a} = -\frac{D}{a^3}\{f'''(1) - (2-\nu)(m\pi)^2 f'(1)\}\sin\frac{m\pi y}{a}. \end{aligned}\right\} \tag{16}$$

At this stage it is convenient to introduce the notation

$$\chi_1(m) = \frac{1 + \dfrac{3-\nu}{1+\nu}\dfrac{\sinh 2m\pi}{2m\pi}}{\left(\dfrac{3-\nu}{1+\nu}\dfrac{\sinh m\pi}{m\pi}\right)^2 - 1} \tag{17}$$

$$\chi_2(m) = (m\pi)^2 \frac{\left[\dfrac{(3-\nu)(1-\nu)}{(1+\nu)^2}\left(\dfrac{\sinh m\pi}{m\pi}\right)^2 - 1\right]}{\left(\dfrac{3-\nu}{1+\nu}\dfrac{\sinh m\pi}{m\pi}\right)^2 - 1}. \tag{18}$$

Equations (11), (12) and (16) may now be substituted into equations (14) and (15) to give

$$-f'''(1) + (2-\nu)(m\pi)^2 f'(1) + \frac{4Gha^2\tan^2\theta}{D(1+\nu)}\left[\chi_1 + \frac{(1+\nu)}{2}\frac{c_1}{c_0}\chi_2\right]\left[f(1) + \frac{b}{a}f'(1)\right] - \\ - \frac{Pa(m\pi)^2\left[f(1) + \dfrac{b}{3a}f'(1)\right]}{2D\cos^2\theta} + \frac{EI(m\pi)^4\left[f(1) + \dfrac{b}{3a}f'(1)\right]}{2Da\cos^2\theta} = 0 \tag{19}$$

and

$$f''(1) - \nu(m\pi)^2 f(1) + \frac{1}{3}\frac{b}{a}(1+2\sin^2\theta)[f'''(1) - (2-\nu)(m\pi)^2 f'(1)] + \\ + \frac{8b}{3a}\frac{Gha^2\sin^2\theta}{D(1+\nu)}\left[\chi_1 - \frac{(1+\nu)}{4}\frac{c_1}{c_0}\chi_2\right]\left[f(1) + \frac{b}{a}f'(1)\right] + \frac{GJ(m\pi)^2}{2Da}f'(1) = 0. \tag{20}$$

If θ is assumed small, the various parameters can be written in terms of c_0/h, c_1/c_0 and k (the ratio of the compressive stress in the fillet to the spanwise compressive stress in the skin) as follows:

$$\left.\begin{aligned} \frac{EI\sec^2\theta}{2Da} &= (1-\nu^2)\left(\frac{c_1}{c_0}\right)^4\left(\frac{c_0}{h}\right)^3 = \left(\frac{1+\nu}{2}\right)\frac{GJ\sec^2\theta}{2Da} \\ \frac{aP\sec^2\theta}{2D} &= \frac{kp^2}{2}\left(\frac{c_1}{c_0}\right)^2\frac{c_0}{h} \\ \text{and}\quad \frac{4Gha^2\tan^2\theta}{D(1+\nu)} &= 24\left(\frac{1-\nu}{1+\nu}\right)\left(\frac{c_0}{h}\right)^2. \end{aligned}\right\} \tag{21}$$

Now if the further non-dimensional parameters

$$\left.\begin{aligned}
-\lambda_1 &= 24\left(\frac{1-\nu}{1+\nu}\right)\frac{c_1}{c_0}\left(\frac{c_0}{h}\right)^2\chi_1 + 12(1-\nu)\left(\frac{c_1}{c_0}\right)^2\left(\frac{c_0}{h}\right)^2(m\pi)^2\chi_2 + \\
&\quad + \frac{k}{6}\left(\frac{c_1}{c_0}\right)^3\frac{c_0}{h}(m\pi)^2\psi^2 - \frac{1-\nu^2}{3}\left(\frac{c_1}{c_0}\right)^5\left(\frac{c_0}{h}\right)^3(m\pi)^4, \\
\lambda_2 &= \frac{k}{2}\left(\frac{c_1}{c_0}\right)^2\left(\frac{c_0}{h}\right)(m\pi)^2\psi^2 - (1-\nu^2)\left(\frac{c_1}{c_0}\right)^4\left(\frac{c_0}{h}\right)^3(m\pi)^4 - \\
&\quad - 24\left(\frac{1-\nu}{1+\nu}\right)\left(\frac{c_0}{h}\right)^2\chi_1 - 12(1-\nu)\frac{c_1}{c_0}\left(\frac{c_0}{h}\right)^2(m\pi)^2\chi_2, \\
-\lambda_3 &= \frac{(2-\nu)}{3}\frac{c_1}{c_0}(m\pi)^2 - 16\left(\frac{1-\nu}{1+\nu}\right)\left(\frac{c_1}{c_0}\right)^2\left(\frac{c_0}{h}\right)^2\chi_1 + \\
&\quad + 4(1-\nu)\left(\frac{c_1}{c_0}\right)^3\left(\frac{c_0}{h}\right)^2(m\pi)^2\chi_2 - 2(1-\nu)\left(\frac{c_1}{c_0}\right)^4\left(\frac{c_0}{h}\right)^3(m\pi)^2 \\
\text{and}\quad \lambda_4 &= 16\left(\frac{1-\nu}{1+\nu}\right)\frac{c_1}{c_0}\left(\frac{c_0}{h}\right)^2\chi_1 - 4(1-\nu)\left(\frac{c_1}{c_0}\right)^2\left(\frac{c_0}{h}\right)^2(m\pi)^2\chi_2,
\end{aligned}\right\} \tag{22}$$

are introduced, equations (21) may be used to express equations (19) and (20) in the form

$$f''' - (2-\nu)(m\pi)^2 f' + \lambda_1 f' + \lambda_2 f = 0 \tag{23}$$

and

$$\frac{c_1}{3c_0}f''' + f'' + \lambda_3 f' - \nu(m\pi)^2 f + \lambda_4 f = 0. \tag{24}$$

Substitution of the expression for f given by equation (10) into these equations gives

$$\left.\begin{aligned}
X_1 A + X_2 B &= 0 \\
\text{and}\quad X_3 A + X_4 B &= 0
\end{aligned}\right\} \tag{25}$$

where

$$\left.\begin{aligned}
X_1 &= \alpha t \sinh\alpha - \beta s \sin\beta + \lambda_1(\alpha\sinh\alpha + \beta\sin\beta) + \lambda_2(\cosh\alpha - \cos\beta), \\
X_2 &= t\cosh\alpha + s\cos\beta + \lambda_1(\cosh\alpha - \cos\beta) + \lambda_2\left(\frac{\sinh\alpha}{\alpha} - \frac{\sin\beta}{\beta}\right) \\
X_3 &= s\cosh\alpha + t\cos\beta + \frac{1}{3}\frac{c_1}{c_0}(\alpha^3\sinh\alpha - \beta^3\sin\beta) + \\
&\quad + \lambda_3(\alpha\sinh\alpha + \beta\sin\beta) + \lambda_4(\cosh\alpha - \cos\beta) \\
\text{and}\quad X_4 &= \frac{s\sinh\alpha}{\alpha} + \frac{t\sin\beta}{\beta} + \frac{1}{3}\frac{c_1}{c_0}(\alpha^2\cosh\alpha + \beta^2\cos\beta) + \\
&\quad + \lambda_3(\cosh\alpha - \cos\beta) + \lambda_4\left(\frac{\sinh\alpha}{\alpha} - \frac{\sin\beta}{\beta}\right),
\end{aligned}\right\} \tag{26}$$

s and t being given by

$$\left.\begin{aligned}
s &= \alpha^2 - \nu(m\pi)^2 \\
\text{and}\quad t &= \beta^2 + \nu(m\pi)^2.
\end{aligned}\right\} \tag{27}$$

The condition for buckling is that the values of A and B obtained from equations (25) should be non-zero, so that

$$\begin{vmatrix} X_1 X_2 \\ X_3 X_4 \end{vmatrix} = 0. \tag{28}$$

Equation (28) is an equation of the form

$$R\left(\frac{c_0}{h}, \frac{c_1}{c_0}, k, m\pi, \psi\right) = 0, \tag{29}$$

where in any given example c_0/h, c_1/c_0 and k are known. To determine the onset of buckling, equation (29) must be solved for ψ for a range of values of m and the smallest value of ψ chosen.

4. *The Numerical Evaluation of the Buckling Stress.* The calculation of the critical value of ψ from the buckling condition given by equations (25) and (26) was programmed for the Royal Aircraft Establishment, Mercury digital computer.

The first root of equation (29) was determined for a given value of $m\pi$ to an accuracy of $0 \cdot 001$ (corresponding to about $0 \cdot 02\%$) and the value of $m\pi$ which gave the smallest of these roots was evaluated to an accuracy of $0 \cdot 0625$ (corresponding to about $1\frac{1}{2}\%$). The final value of ψ_{cr} obtained was correct at worst to $0 \cdot 005$ (about $0 \cdot 1\%$) because the value of the root varied slowly with $m\pi$. A further programme was made to evaluate the deflected shape of the skin, the bending moment and the vertical force at six stations equally spaced along the skin. The results obtained from these programmes are shown in Figs. 2 to 11 inclusive.

5. *Discussion of Results.* The buckling parameter ψ_{cr} was calculated for values of c_1/c_0 varying between $0 \cdot 1$ and 1 and values of c_0/h not exceeding 20. The smallest practical value of c_0/h depends on the value of c_1/c_0 because c_1 must be greater than h. The calculations were performed for values of k equal to -1, 0, 1 and 2 and the results are shown in Figs. 2 to 5. The variation of spanwise wavelength over the same ranges of c_1/c_0 and c_0/h and k is shown in Figs. 6 to 9. It can be seen that for certain values of c_1/c_0 and k there are discontinuities in the wavelength as c_0/h increases, and corresponding discontinuities in the slope of the buckling-parameter curves. At these discontinuities there are two possible modes of buckling, one very similar to the clamped-clamped plate and the other with longer spanwise waves.

Fig. 9 shows the variation of ψ with wavelength for some particular values of c_0/h, c_1/c_0 and k, one set of these parameters being chosen to be at a point of discontinuity.

In the analysis no account is taken of the effect of chordwise ribs on the stiffness of the structure. If however there are ribs spaced at distances less than about $1 \cdot 5l$, where l is the spanwise half-wavelength of the buckled mode with no ribs present, the half-wavelength of the mode actually adopted is in general equal to the rib spacing. Thus Fig. 9 can be used to obtain an estimate of the effect of closely-spaced ribs for a number of examples. In those cases where two alternative modes exist for similar buckling loads, that with the shorter wavelength is likely to be adopted if ribs are present, and thus while having a large effect on the mode of buckling they cause little change in the critical load. In most cases the effect of ribs is small provided the distance between them is greater than three times the distance between the fillet and the first spar. However, if the stress in the fillet is high compared to that in the skin, the spanwise waves become long and the presence of ribs leads to a significant increase in the buckling load.

Fig. 10 shows for a particular example $c_1/c_0 = 0 \cdot 6$ and $k = 1$, the variation of deflection, bending moment and vertical force across the width of the skin for different values of c_0/h. The two distinct types of mode which occur on either side of the discontinuity of wavelength (*see* Fig. 6) can be seen.

Figs. 11 and 12 show dimensions of five possible leading edges. The critical spanwise stresses for these are given in Table 1 for the four values of k previously mentioned.

To show the order of temperature rise at which buckling takes place it is assumed that the leading edge is subjected to a constant temperature rise ΔT above the rest of the wing (shown in Fig. 12c) and that the central portion of the wing is perfectly rigid. This means that the thermal stress throughout the leading edge is $\alpha E \Delta T$. Critical temperatures based on this law are given in Table 1 (corresponding to stresses for $k = 1$). This is likely to be an underestimate of the critical temperatures occurring in practice, and for more accurate prediction the design of the whole wing must be taken into account.

Fig. 13 shows the variation of effective torsional rigidity of the fillet with spanwise wavelength and end stress. The parameters used in Fig. 13 may be expressed in the notation of the main body of the report as

$$\psi_1^2 = \frac{k}{4} \frac{\psi_{cr}^2}{(c_0/h)^2}$$

$$m_1 \pi = \frac{\pi(c_1/c_0)}{(l/a)} .$$

Thus for any set of values of c_0/h, c_1/c_0 and k, an approximate value of the factor that should have been applied to the torsional rigidity of the fillet may be obtained. Now for the five examples given in Table 1, that of Fig. 12b involves the largest error of this type and for this case the required factor is about $0 \cdot 70$ when $k = 1$. Since the torsional rigidity of the fillet is itself only one of several factors influencing the buckling load, the error entailed in using the St. Venant value is small.

6. *Conclusions.* An analysis has been given of the buckling under spanwise thermal stress of the leading edge of a built-up wing. Graphs have been presented showing the buckling parameter over a wide range of leading-edge dimensions. Examples have been given showing critical temperatures and stresses for some possible leading edges.

NOTATION

E, ν	Young's modulus and Poisson's ratio
X, Y, W	Chordwise and spanwise co-ordinates and deflection perpendicular to mid-chord
x, y, z, w	Co-ordinates relative to skin and deflection in positive z-direction, (*see* Fig. 1c)
u, v	Displacements of skin in x- and y-directions respectively
a, b, θ, c_0, c_1, h	Dimensions shown in Fig. 1a
V_x, M_x, F	Forces and couple shown in Fig. 1b
S	Spanwise shear force on $x = a$
M_T	Moment on fillet due to S
V_T	Resultant vertical force on fillet arising from M_T
N_y/h	Spanwise compressive thermal stress in skin
kN_y/h	Spanwise thermal stress on fillet
D	Flexural rigidity of skin
EI, GJ	Flexural and torsional rigidities of fillet respectively
P	End load on fillet
ψ	$= \sqrt{\left(\frac{N_y a^2}{D}\right)}$
$f(x/a) \sin \frac{m\pi y}{a}$	Function defining deflection of skin
l	$= a/m$, half wavelength of buckles in the spanwise direction
α^2, β^2	Defined by equation (8)
χ_1, χ_2	Defined by equations (17) and (18)
λ_1, λ_2, λ_3, λ_4	Defined by equation (22)
s, t	Defined by equation (27)
X_1, X_2, X_3, X_4	Defined by equation (26)
R	$= X_1X_4 - X_2X_3$

REFERENCES

No.	*Author*	*Title, etc.*
1	.. .. ..	Roy. Aero. Soc. Structures Data Sheets Series 00.03.
2	E. H. Mansfield	Leading-edge buckling due to aerodynamic heating. A.R.C. R. & M. 3197. May, 1959.
3	S. Timoshenko	*Theory of elastic stability.* McGraw-Hill. 1936.
4	S. Timoshenko and J. N. Goodier ..	*Theory of elasticity.* 2nd Edition, McGraw-Hill. 1951.

NOTATION

Used only in Appendix I

p	=	$m\pi$
A	=	$\left[f(1) + \frac{b}{a} f'(1)\right] \tan \theta$
ζ	=	$\frac{x}{a} + i \frac{y}{a}$
B	=	$u + iv$
$\sigma_x, \sigma_y, \tau_{xy}$		Stresses in skin arising due to tip deflection
Θ	=	$\sigma_x + \sigma_y$
Φ	=	$\sigma_x - \sigma_y + 2i\tau_{xy}$
$\Omega(\zeta), \omega(\zeta)$		Complex stress functions

APPENDIX I

The Distribution of Plane Stress in the Skin

As explained in Section 3, when the leading edge of the wing deflects, the skin undergoes a displacement in its own plane which gives rise to a state of plane stress. The problem corresponds to that of an infinite strip with zero displacement along one edge and along the other a sinusoidal displacement perpendicular to the edge.

That is

$$\left.\begin{aligned} u &= 0, & v &= 0 \text{ on } x = 0 \\ u &= A \sin\frac{py}{a}, & v &= 0 \text{ on } x = a \end{aligned}\right\} \tag{30}$$

where in this case

$$\left.\begin{aligned} A &= \left[f(1) + \frac{b}{a}f'(1)\right] \tan\theta \\ p &= m\pi\,. \end{aligned}\right\} \tag{31}$$

Now if the complex displacement is given by

$$\left.\begin{aligned} B &= u + iv \\ \zeta &= \frac{x}{a} + i\frac{y}{a}, \end{aligned}\right\} \tag{32}$$

and

the displacement at any point is given by

$$8GB = \frac{3-\nu}{1+\nu}\,\Omega(\zeta) - \zeta\overline{\Omega}'(\bar{\zeta}) - \overline{\omega}'(\bar{\zeta}) \tag{33}$$

where $\Omega(\zeta)$ and $\omega(\zeta)$ are the complex potential functions satisfying the boundary conditions. The stresses are given by the equations

$$\left.\begin{aligned} \Theta &= \sigma_x + \sigma_y = \frac{1}{2a}\,[\Omega'(\zeta) + \overline{\Omega}'(\bar{\zeta})] \\ \Phi &= \sigma_x - \sigma_y + 2i\tau_{xy} = -\frac{1}{2a}\,[\zeta\overline{\Omega}''(\bar{\zeta}) + \overline{\omega}''(\bar{\zeta})]\,. \end{aligned}\right\} \tag{34}$$

and

Consider the potential functions

$$\Omega(\zeta) = -\frac{4AGi\left[\cosh p(\zeta-1) + \left(\dfrac{3-\nu}{1+\nu}\right)\dfrac{\sinh p}{p}\cosh p\zeta\right]}{p\left[\left(\dfrac{3-\nu}{1+\nu}\dfrac{\sinh p}{p}\right)^2 - 1\right]} \tag{35}$$

and

$$\overline{\omega}'(\bar{\zeta}) = -\frac{4AGi\left[\dfrac{3-\nu}{1+\nu}\cosh p(\bar{\zeta}+1) + \left(\dfrac{3-\nu}{1+\nu}\right)^2\dfrac{\sinh p}{p}\cosh p\bar{\zeta} - p\bar{\zeta}\left\{\sinh p(\bar{\zeta}-1) + \left(\dfrac{3-\nu}{1+\nu}\right)\dfrac{\sinh p}{p}\sinh p\bar{\zeta}\right\}\right]}{p\left[\left(\dfrac{3-\nu}{1+\nu}\dfrac{\sinh p}{p}\right)^2 - 1\right]}\,.$$

Substituting these expressions into equation (33) the displacement is given by

$$8GB = -\frac{4AGi\left[\left(\frac{3-\nu}{1+\nu}\right)\{\cosh p(\zeta-1)-\cosh p(\bar{\zeta}+1)\}+\left(\frac{3-\nu}{1+\nu}\right)^2\frac{\sinh p}{p}\{\cosh p\zeta-\cosh p\bar{\zeta}\}+ + p(\zeta+\bar{\zeta})\left\{\sinh p(\bar{\zeta}-1)+\left(\frac{3-\nu}{1+\nu}\right)\frac{\sinh p}{p}\sinh p\bar{\zeta}\right\}\right]}{p\left[\left(\frac{3-\nu}{1+\nu}\frac{\sinh p}{p}\right)^2-1\right]}.$$

On $x = 0$, where $\zeta = iy/a$, this expression becomes zero, and on $x = a$, where $\zeta = 1 + (iy/a)$ it reduces to $B = A \sin py$. Therefore the above potential functions are the solution to the problem. Now to find the stresses on $x = a$, these potentials must be substituted into equations (34) and the boundary condition $x = a$ applied. The expressions derived in this way are

$$\left.\begin{aligned}
(\sigma_x)_{x=a} &= \frac{4G}{a(1+\nu)}\left[\frac{1+\left(\frac{3-\nu}{1+\nu}\right)\frac{\sinh 2p}{2p}}{\left(\frac{3-\nu}{1+\nu}\frac{\sinh p}{p}\right)^2-1}\right]A\sin p\frac{y}{a}\\
(\sigma_y)_{x=a} &\doteq \nu(\sigma_x)_{x=a}\\
(\tau_{xy})_{x=a} &= \frac{2Gp}{a}\left[\frac{\frac{(3-\nu)(1-\nu)}{(1+\nu)^2}\left(\frac{\sinh p}{p}\right)^2-1}{\left(\frac{3-\nu}{1+\nu}\frac{\sinh p}{p}\right)^2-1}\right]A\cos p\frac{y}{a}.
\end{aligned}\right\} \qquad (36)$$

The effect of the stresses σ_x and τ_{xy} on the boundary condition at $x = a$ is shown in Section 3.

NOTATION

Used only in Appendix II

b		Width of plate
h_1		Maximum thickness of plate
$M \sin \frac{m_1 \pi y}{b}$		Applied edge moment
σ_1		Applied end stress
w_1	$=$	$h_1 f_1 \left(\frac{x}{b}\right) \sin \frac{m_1 \pi y}{b}$, downward deflection of plate
D_1	$=$	$E h_1^3/12(1-\nu^2)$
ψ_1^2	$=$	$\sigma_1 h_1 b^2/D_1$
μ	$=$	$Mb^2/h_1 D_1$
η		Ratio of effective torsional rigidity of plate to St. Venant value
V		Total potential energy of plate
$\bar{V}$	$=$	$\frac{4b^2 m_1 V}{D_1 h_1^2}$
U		Strain energy of plate
W_M		Energy due to applied moment
W_{σ_1}		Energy due to end stress
a_0, a_1, A_0, A_1		Arbitrary constants in expressions for f_1
$\alpha_0, \alpha_1, \alpha_2$		Defined by equation (50)
$\beta_0, \beta_1, \beta_2, \gamma_0, \gamma_1, \gamma_2$		Defined by equation (52)

APPENDIX II

The Effective Torsional Rigidity of the Fillet

In calculating the buckling load, the torsional rigidity of the fillet is assumed to have the value given by St. Venant theory. However this value is altered by the finite wavelength of the buckles and the end stress in the fillet. An estimate of the effective torsional rigidity of the fillet can be obtained by considering a tapered plate of width b and maximum thickness h_1 with sinusoidally-distributed edge moment $M \sin (m_1 \pi y/b)$, and constant end stress σ_1 (*see* Fig. 13). Now if w_1 is the downward deflection of the plate and x is measured from the tip across the width, the ratio of the effective torsional rigidity at the point of attachment of the skin to the St. Venant value is

$$\eta = + \frac{12}{G h_1^3 b} \frac{M \sin \dfrac{m_1 \pi y}{b}}{\left(\dfrac{\partial^3 w_1}{\partial x \partial y^2}\right)_{x=b}} . \tag{37}$$

If w_1 is taken as

$$w_1 = h_1 f_1 \left(\frac{x}{b}\right) \sin \frac{m_1 \pi y}{b}, \tag{38}$$

equation (37) becomes

$$\eta = - \frac{12 M b^2}{h_1^4 G (m_1 \pi)^2 f_1'(1)} . \tag{39}$$

Now an approximate solution to this problem can be obtained using the Ritz method. The total potential energy of the system is

$$V = U + W_M + W_{\sigma_1} \tag{40}$$

where

U = the strain energy of deformation per half-wave

$$= \frac{1}{2} \int_0^b \int_0^{b/m_1} \left(\frac{x}{b}\right)^3 D_1 \left\{ \left(\frac{\partial^2 w_1}{\partial x^2} + \frac{\partial^2 w_1}{\partial y^2} \right)^2 + 2(1-\nu) \left[\left(\frac{\partial^2 w_1}{\partial x \partial y} \right)^2 - \frac{\partial^2 w_1}{\partial x^2} \frac{\partial^2 w_1}{\partial y^2} \right] \right\} dy \tag{41}$$

W_M = energy due to the edge moment per half-wave

$$= \int_0^{b/m_1} M \sin \frac{m_1 \pi y}{b} \left(\frac{\partial w_1}{\partial x}\right)_{x=b} dy \tag{42}$$

and

$W_{\sigma 1}$ = energy due to the end stress per half-wave

$$= - \frac{1}{2} \int_0^b \int_0^{b/m_1} \sigma_1 h_1 \left(\frac{x}{b}\right) \left(\frac{\partial w_1}{\partial y}\right)^2 dx\, dy . \tag{43}$$

Now writing

$$\left.\begin{aligned} \xi &= \frac{x}{b}, & D_1 &= \frac{E h_1^2}{12(1-\nu^2)}, \\ \psi_1^2 &= \frac{\sigma_1 h_1 b^2}{D_1}, & \mu &= \frac{M b^2}{h_1 D_1}, \\ \bar{V} &= \frac{4 b^2 m_1 V}{D_1 h_1^2}, \end{aligned}\right\} \tag{44}$$

and

equations (40) to (43) become on substitution of equation (38), and integration with respect to y,

$$\bar{V} = \int_0^1 \xi^3 \left\{ (f_1'')^2 - 2\nu(m_1\pi)^2 f_1 f_1'' + 2(1-\nu)(m_1\pi)^2 (f_1')^2 + \right.$$
$$\left. + (m_1\pi)^2 \left[(m_1\pi)^2 - \frac{\psi_1^2}{\xi^2} \right] f_1^2 \right\} d\xi + 2\mu f_1'(1) \tag{45}$$

and

$$\eta = -\frac{2\mu}{(1-\nu)(m_1\pi)^2 f'(1)}. \tag{46}$$

The problem is now reduced to finding an expression for $f_1(\xi)$ which minimises $\bar{V}$. Two types of solution were tried, a parabolic type

$$f_1(\xi) = (a_0 + a_1\xi)(1-\xi) \tag{47}$$

which was found to be better for small values of $m_1\pi$ (i.e., large wavelengths), and an exponential type

$$f_1(\xi) = A_0(1-\xi)e^{-A_1(1-\xi)} \tag{48}$$

which was found to be better for large values of $m_1\pi$. In fact as $m_1\pi$ tends to infinity this solution tends to the exact one.

These solutions were substituted into equation (45), the integrations performed and simultaneous equations for the arbitrary constants obtained by differentiating with respect to each arbitrary constant and equating the result to zero. In the first case this leads to an explicit expression for η,

$$\eta = \frac{1}{1-\nu} \frac{[\alpha_0\alpha_2 - (m_1\pi)^2\alpha_1^2]}{[\alpha_2 + (m_1\pi)^2\alpha_0 - 2(m_1\pi)^2\alpha_1]} \tag{49}$$

where

$$\left.\begin{aligned} \alpha_0 &= 1 - \nu + \frac{(m_1\pi)^2}{30} - \frac{\psi_1^2}{6} \\ \alpha_1 &= \frac{3-2\nu}{5} + \frac{2}{105}(m_1\pi)^2 - \frac{\psi_1^2}{15} \\ \alpha_2 &= 2 + \frac{7-3\nu}{15}(m_1\pi)^2 + \frac{1}{84}(m_1\pi)^4 - \frac{(m_1\pi)^2\psi_1^2}{30} \end{aligned}\right\} \tag{50}$$

whereas in the second case it is necessary to solve a transcendental equation for A_2,

$$(\gamma_0 - \beta_0)I_3(2A_1) + (\beta_0 + \gamma_1 - \beta_1)I_4(2A_1) + (\beta_1 - \gamma_2 + \beta_2)I_5(2A_1) +$$
$$+ \beta_2 I_6(2A_1) - (m_1\pi)^2\psi_1^2[I_2(2A_1) - 2I_3(2A_1) + I_4(2A_1)] = 0 \tag{51}$$

where

$$\left.\begin{aligned} I_n(x) &= \int_0^1 t^n e^{-(1-x)t} dt \\ \beta_0 &= A_1^2(A_1-2)^2 - 2\nu(m_1\pi)^2 A_1(A_1-2) + 2(1-\nu)(m_1\pi)^2(A_1-1)^2 + (m_1\pi)^4 \\ \beta_1 &= -2[A_1^3(A_1-2) + 2(1-2\nu)(m_1\pi)^2 A_1(A_1-1) + (m_1\pi)^4] \\ \beta_2 &= A_1^4 + 2(1-2\nu)A_1^2(m_1\pi)^2 + (m_1\pi)^4 \\ \gamma_0 &= 2(A_1-1)[A_1(A_1-2) + (1-2\nu)(m_1\pi)^2] \\ \gamma_1 &= -2[A_1^2(2A_1-3) + (1-2\nu)(m_1\pi)^2(2A_1-1)] \end{aligned}\right\} \tag{52}$$

and

$$\gamma_2 = 2A_1[A_1^2 + (1-2\nu)(m_1\pi)^2].$$

The smallest positive root of equation (51), $A_1^{(1)}$ (say), is found numerically and since in this case the other equation is simply

$$A_0 = \frac{\mu}{\beta_0 I_3(2A_1) + \beta_1 I_4(2A_1) + \beta_2 I_5(2A_1) - (m_1\pi)^2\psi_1^2[I_1(2A_1) - 2I_2(2A_1) + I_3(2A_1)]} \tag{53}$$

the expression for η is

$$\eta = \frac{2}{(1-\nu)(m_1\pi)^2}\{\beta_0^{(1)}I_3(2A_1^{(1)}) + \beta_1^{(1)}I_4(2A_1^{(1)}) + \beta_2^{(1)}I_5(2A_1^{(1)}) -$$

$$- (m_1\pi)^2\psi_1^2[I_1(2A_1^{(1)}) - 2I_2(2A_1^{(1)}) + I_3(2A_1^{(1)})]\} \tag{54}$$

where $\beta_0^{(1)}$, $\beta_1^{(1)}$ and $\beta_2^{(1)}$ are the values of β_0, β_1, and β_2 corresponding to $A_1^{(1)}$.

The numerical results obtained are shown in Fig. 13, the dotted lines indicating that there are no discontinuities of slope in the exact solution.

It should be noted that the point of interest in the present context is the value of the effective torsional rigidity of the fillet at its junction with the skin and that this tends to zero with the spanwise wavelength. This is because as the wavelength becomes short the disturbance is confined to a small region near the edge of the fillet, and in the limit there is a finite bending moment acting over an infinitely small region which is therefore completely flexible. If however the assumption is made that the fillet cross-section remains undeformed, the torsional rigidity rises with decreasing wavelength.

TABLE 1

Critical Stresses and Temperatures for the Examples Discussed in Section 5 and Shown in Figs. 11 and 12

Example shown in Fig.		11a	11b	11c	12a	12b
h/a		0·0050	0·0083	0·0105	0·0167	0·0250
c_0/h		15·0	8·0	8·8	3·3	2·0
c_1/c_0		0·1	0·2	0·4	0·6	1·0
Critical spanwise compressive stress in lb/in.² for various values of k	$k = -1$	3080	8330	18040	40840	93650
	$k = 0$.	3060	8120	17990	38340	91270
	$k = 1$.	3040	7860	17950	27140	44370
	$k = 2$.	3020	7550	17900	19880	27590
Critical average temperature rise of leading edge in °C assuming $\sigma_{cr} = \alpha E(\Delta T)_{cr}$ . .		10	26	60	90	146

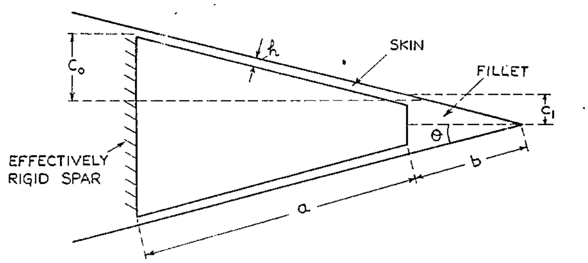

(a) DIAGRAM OF LEADING EDGE SHOWING DIMENSIONS.

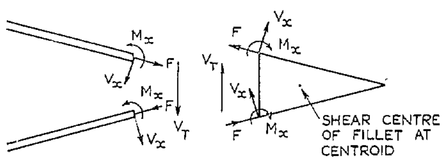

(b) DIAGRAM SHOWING THE FORCES AND MOMENTS ACTING ON THE FILLET.

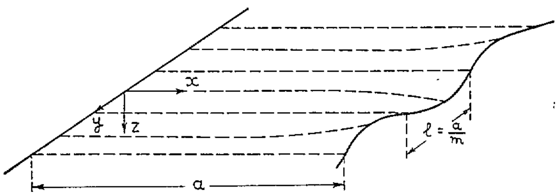

(c) DIAGRAM SHOWING THE CO-ORDINATE SYSTEM USED AND TYPE OF MODE ASSUMED WHEN CONSIDERING THE BUCKLING OF THE SKIN.

FIG. 1a to c. Co-ordinate system and notations used in the analysis.

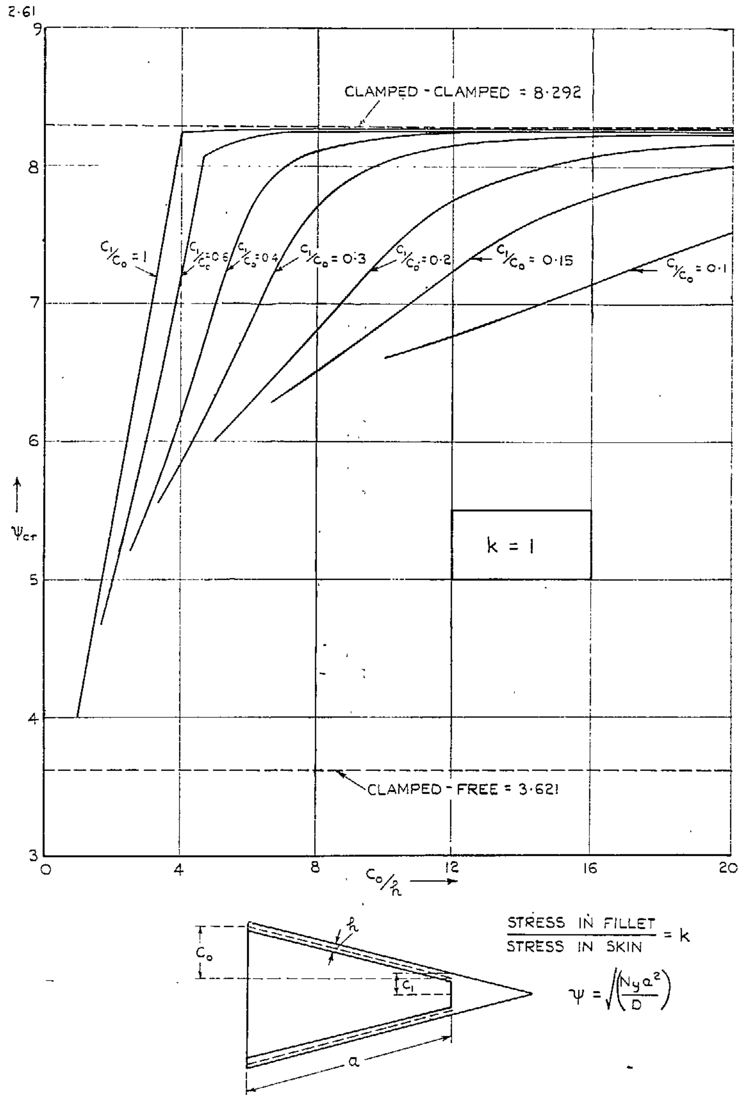

FIG. 2. The variation of the buckling parameter ψ_{cr} with c_0/h for different values of c_1/c_0 when $k = 1$.

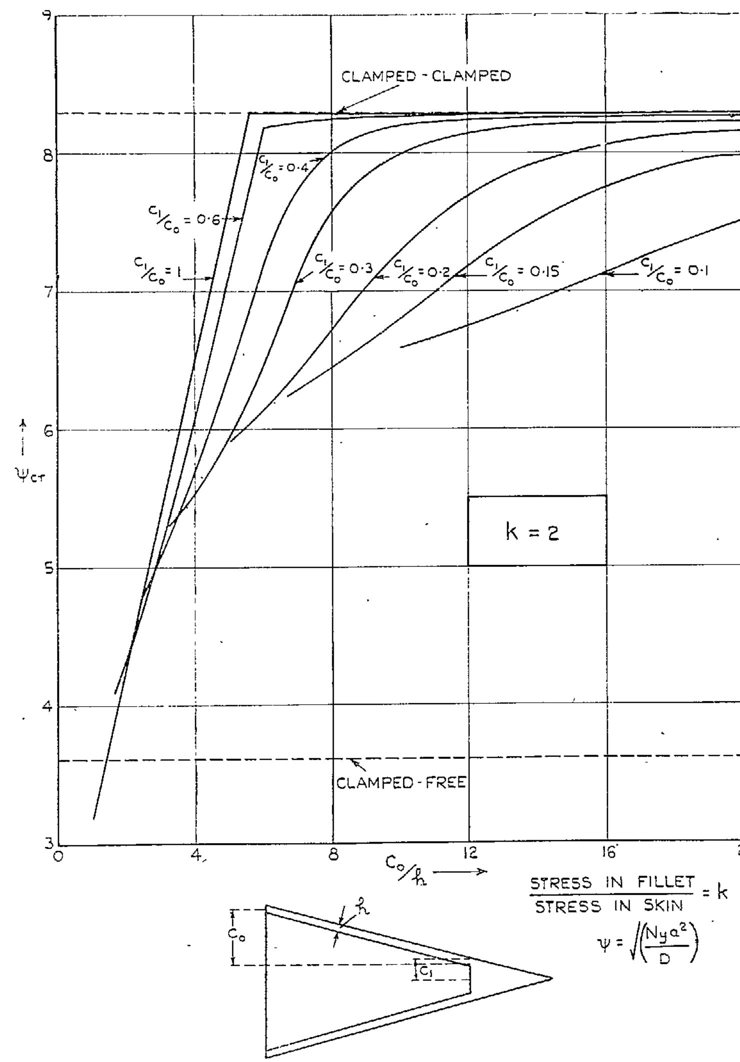

FIG. 3. The variation of the buckling parameter ψ_{cr} with c_0/h for different values of c_1/c_0 when $k = 2$.

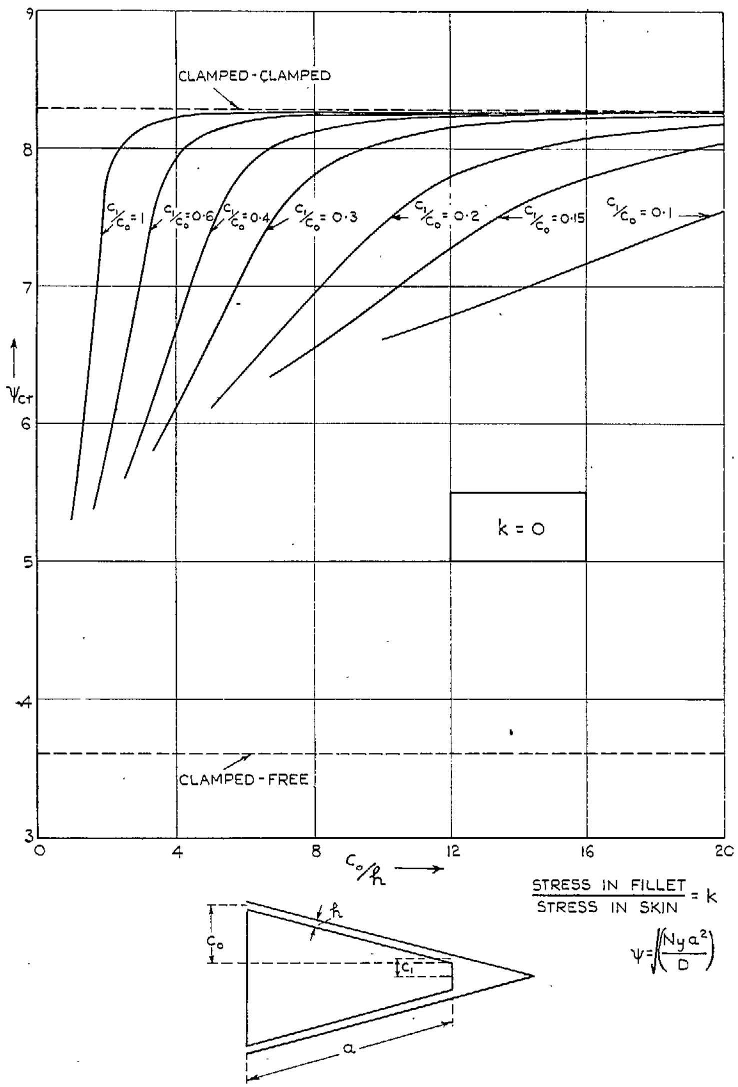

FIG. 4. The variation of the buckling parameter ψ_{cr} with c_0/h for different values of c_1/c_0 when $k = 0$.

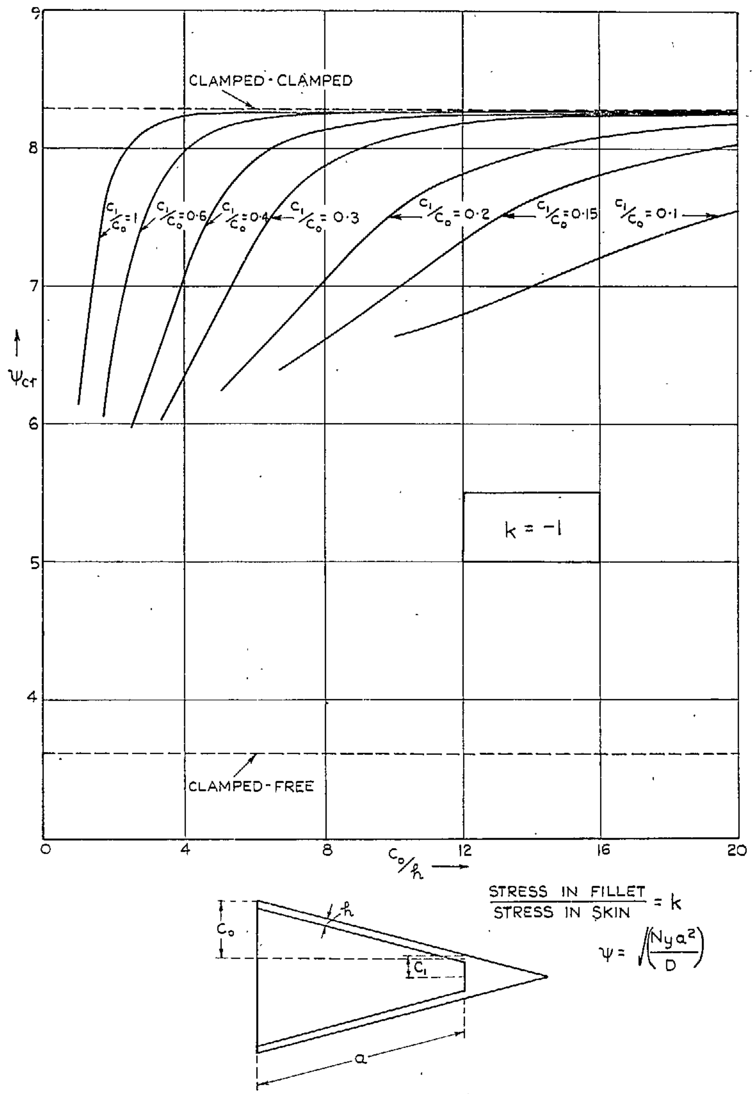

FIG. 5. The variation of the buckling parameter ψ_{cr} with c_0/h for different values of c_1/c_0 when $k = -1$.

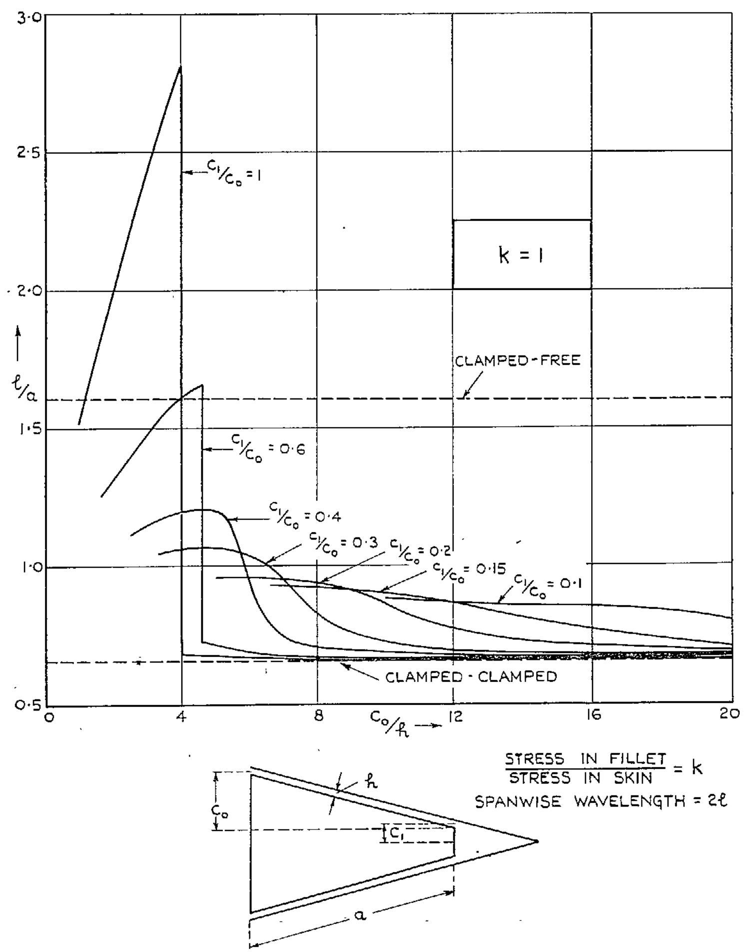

FIG. 6. The variation of spanwise wavelength with c_0/h for different values of c_1/c_0 when $k = 1$.

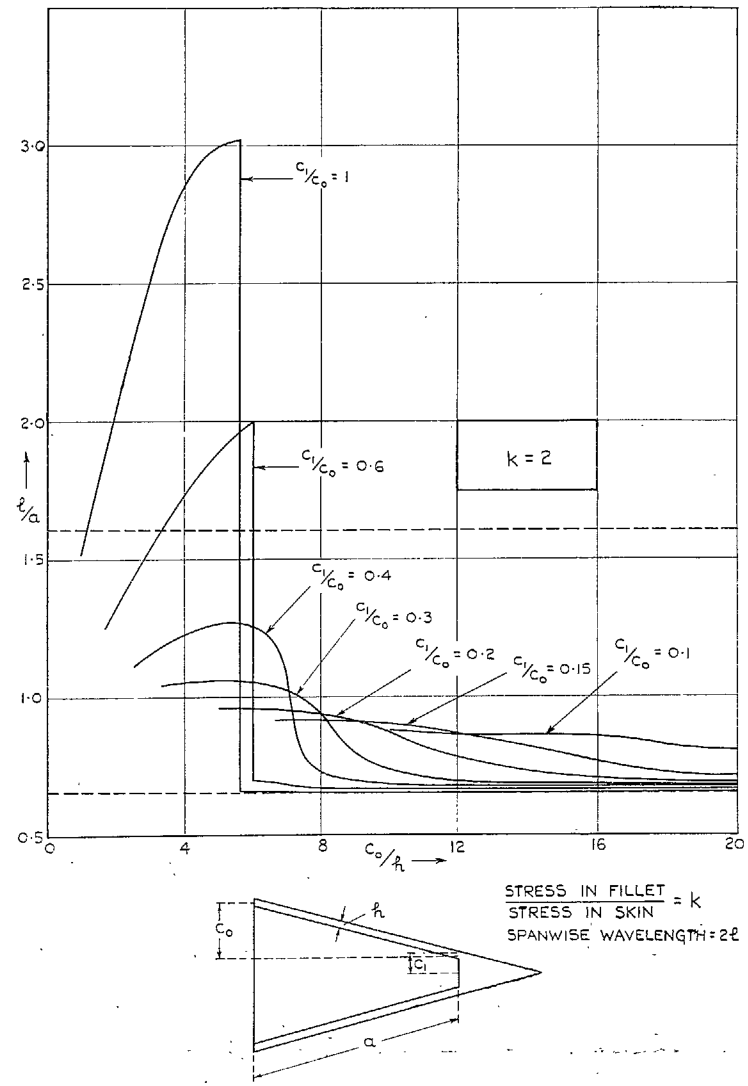

FIG. 7. The variation of spanwise wavelength with c_0/h for different values of c_1/c_0 when $k = 2$.

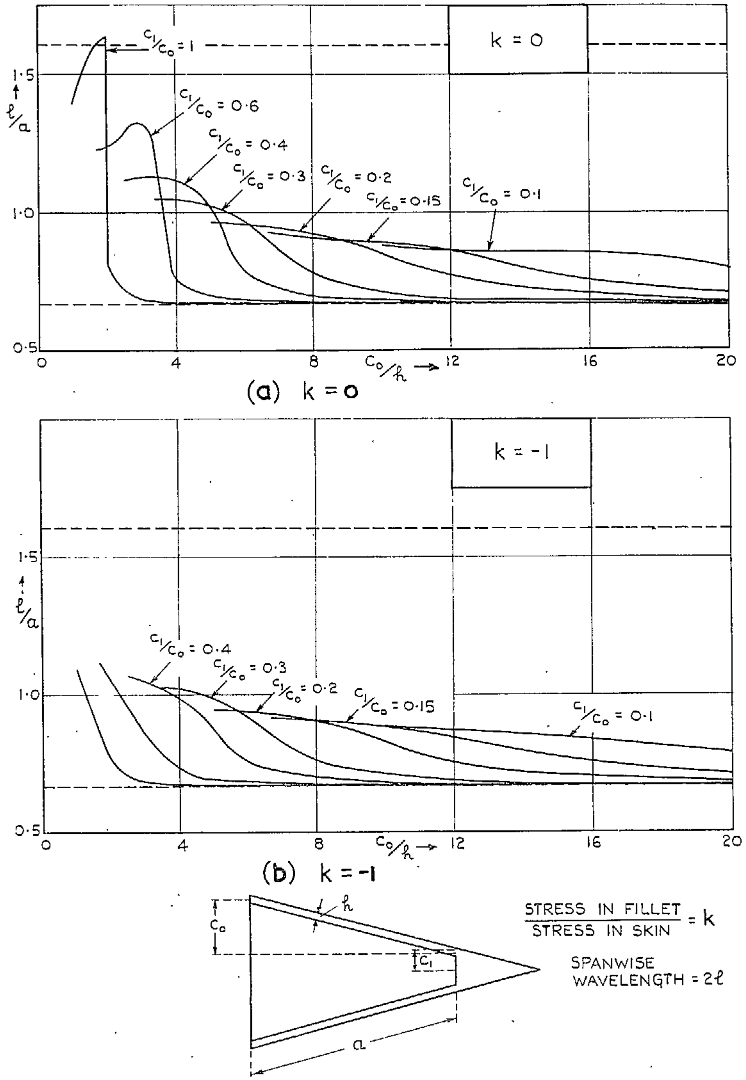

FIG. 8a and b. The variation of spanwise wavelength with c_0/h for different values of c_1/c_0 when $k = 0$ and -1.

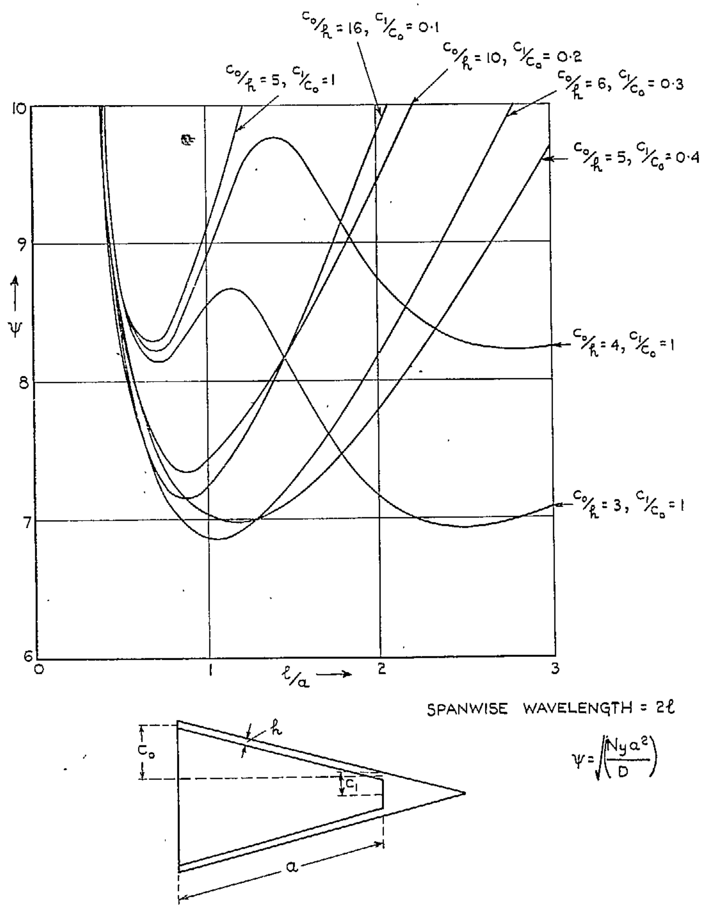

FIG. 9. The variation of buckling load with spanwise wavelength in some examples. In all cases the fillet stress and skin stress are equal.

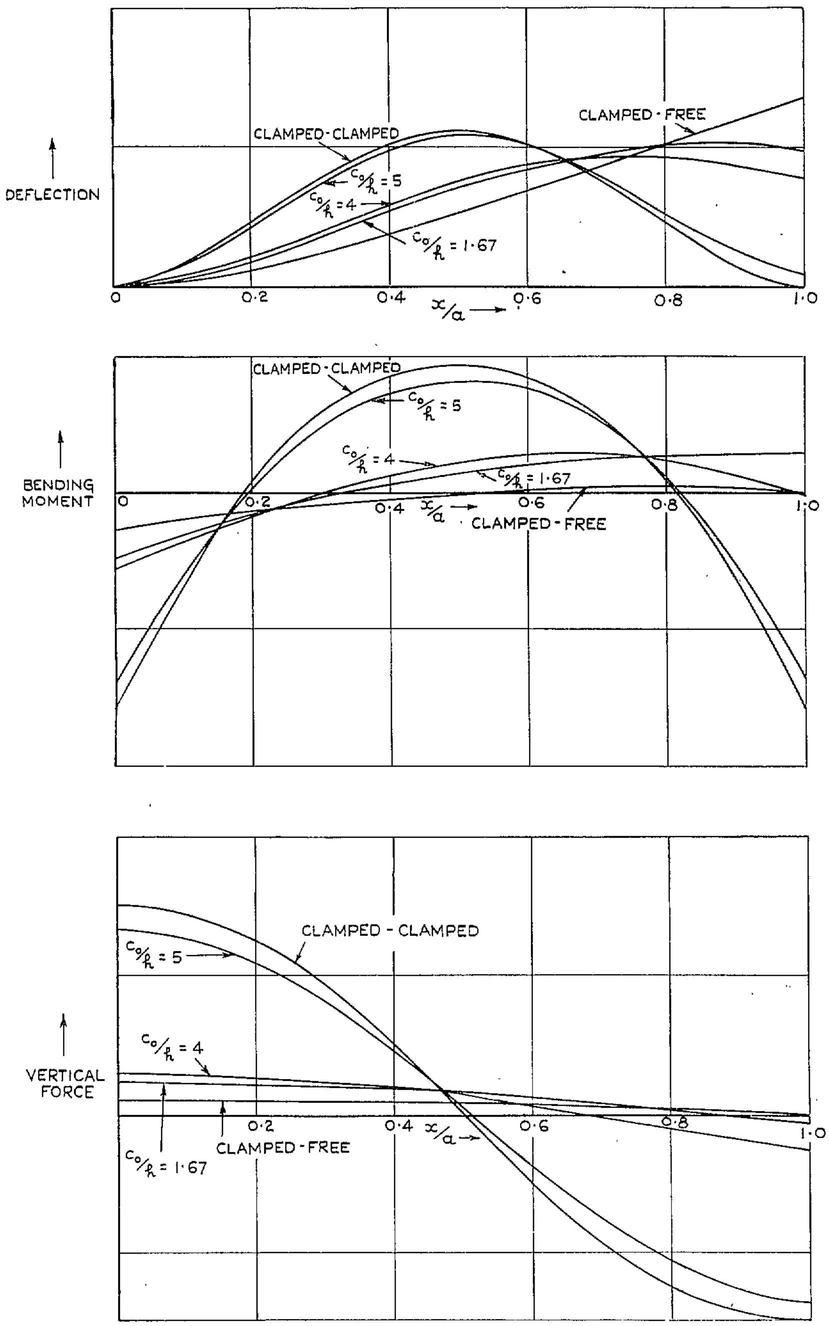

FIG. 10. Diagrams showing variation of deflection, bending moment and vertical force across the width of the skin for different values of c_0/h when $c_1/c_0 = 0·6$ and $k = 1$.

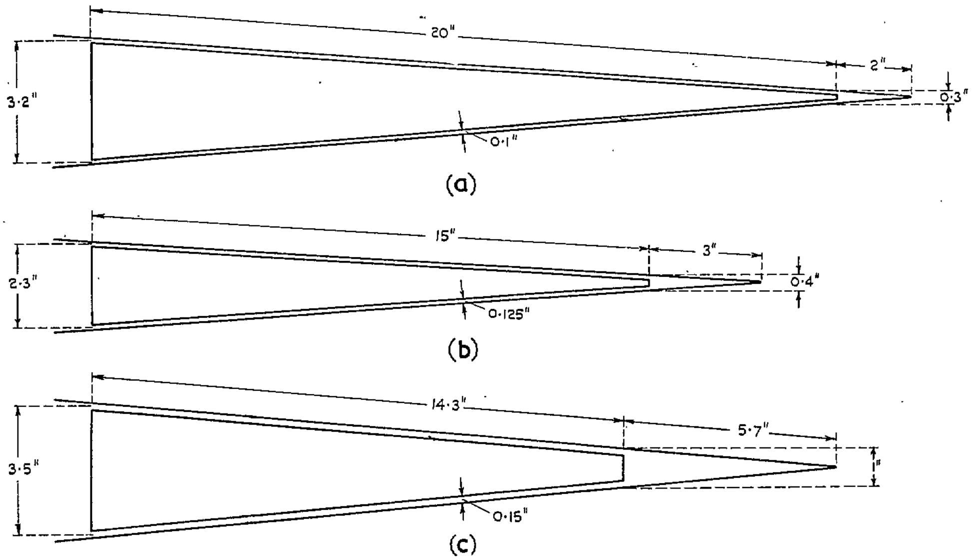

FIG. 11a to c. Some examples of possible leading-edge dimensions.

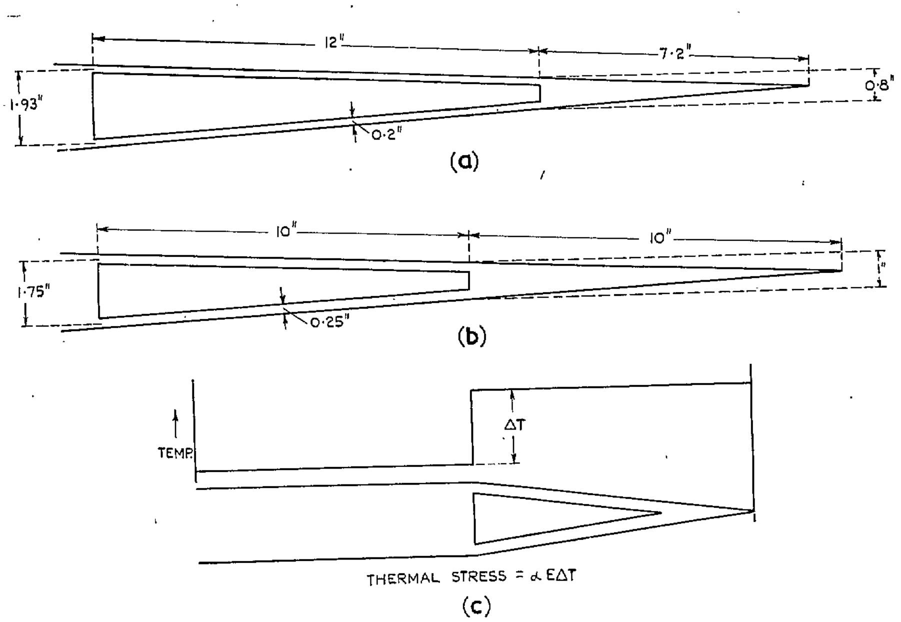

FIG. 12a to c. Two further examples of possible leading-edge dimensions together with diagram of assumed temperature distribution.

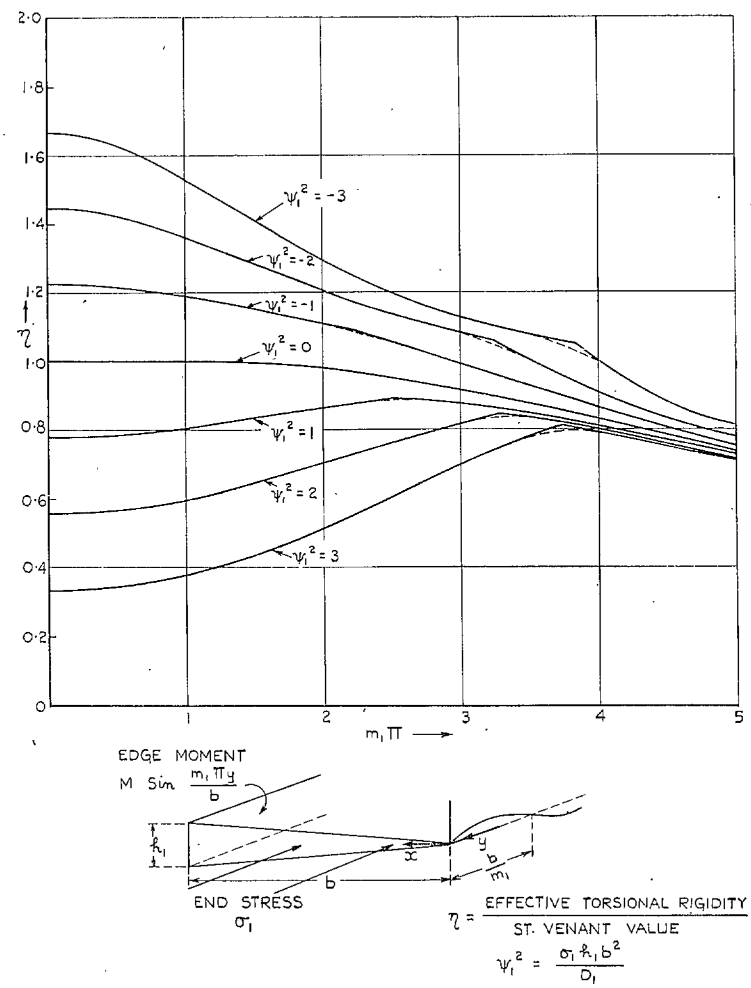

FIG. 13. The effective torsional rigidity of a tapered plate under sinusoidal edge moment and uniform end stress.

(85553) Wt. 64/1857 K.5 11/62 Hw.

Publications of the Aeronautical Research Council

ANNUAL TECHNICAL REPORTS OF THE AERONAUTICAL RESEARCH COUNCIL (BOUND VOLUMES)

1942 Vol. I. Aero and Hydrodynamics, Aerofoils, Airscrews, Engines. 75*s.* (post 2*s.* 9*d.*)
Vol. II. Noise, Parachutes, Stability and Control, Structures, Vibration, Wind Tunnels. 47*s.* 6*d.* (post 2*s.* 3*d.*)

1943 Vol. I. Aerodynamics, Aerofoils, Airscrews. 80*s.* (post 2*s.* 6*d.*)
Vol. II. Engines, Flutter, Materials, Parachutes, Performance, Stability and Control, Structures. 90*s.* (post 2*s.* 9*d.*)

1944 Vol. I. Aero and Hydrodynamics, Aerofoils, Aircraft, Airscrews, Controls. 84*s.* (post 3*s.*)
Vol. II. Flutter and Vibration, Materials, Miscellaneous, Navigation, Parachutes, Performance, Plates and Panels, Stability, Structures, Test Equipment, Wind Tunnels. 84*s.* (post 3*s.*)

1945 Vol. I. Aero and Hydrodynamics, Aerofoils. 130*s.* (post 3*s.* 6*d.*)
Vol. II. Aircraft, Airscrews, Controls. 130*s.* (post 3*s.* 6*d.*)
Vol. III. Flutter and Vibration, Instruments, Miscellaneous, Parachutes, Plates and Panels, Propulsion. 130*s.* (post 3*s.* 3*d.*)
Vol. IV. Stability, Structures, Wind Tunnels, Wind Tunnel Technique. 130*s.* (post 3*s.* 3*d.*)

1946 Vol. I. Accidents, Aerodynamics, Aerofoils and Hydrofoils. 168*s.* (post 3*s.* 9*d.*)
Vol. II. Airscrews, Cabin Cooling, Chemical Hazards, Controls, Flames, Flutter, Helicopters, Instruments and Instrumentation, Interference, Jets, Miscellaneous, Parachutes. 168*s.* (post 3*s.* 3*d.*)
Vol. III. Performance, Propulsion, Seaplanes, Stability, Structures, Wind Tunnels. 168*s.* (post 3*s.* 6*d.*)

1947 Vol. I. Aerodynamics, Aerofoils, Aircraft. 168*s.* (post 3*s.* 9*d.*)
Vol. II. Airscrews and Rotors, Controls, Flutter, Materials, Miscellaneous, Parachutes, Propulsion, Seaplanes, Stability, Structures, Take-off and Landing. 168*s.* (post 3*s.* 9*d.*)

1948 Vol. I. Aerodynamics, Aerofoils, Aircraft, Airscrews, Controls, Flutter and Vibration, Helicopters, Instruments, Propulsion, Seaplane, Stability, Structures, Wind Tunnels. 130*s.* (post 3*s.* 3*d.*)
Vol. II. Aerodynamics, Aerofoils, Aircraft, Airscrews, Controls, Flutter and Vibration, Helicopters, Instruments, Propulsion, Seaplane, Stability, Structures, Wind Tunnels. 110*s.* (post 3*s.* 3*d.*)

Special Volumes

Vol. I. Aero and Hydrodynamics, Aerofoils, Controls, Flutter, Kites, Parachutes, Performance, Propulsion, Stability. 126*s.* (post 3*s.*)
Vol. II. Aero and Hydrodynamics, Aerofoils, Airscrews, Controls, Flutter, Materials, Miscellaneous, Parachutes, Propulsion, Stability, Structures. 147*s.* (post 3*s.*)
Vol. III. Aero and Hydrodynamics, Aerofoils, Airscrews, Controls, Flutter, Kites, Miscellaneous, Parachutes, Propulsion, Seaplanes, Stability, Structures, Test Equipment. 189*s.* (post 3*s.* 9*d.*)

Reviews of the Aeronautical Research Council

1939–48 3*s.* (post 6*d.*) 1949–54 5*s.* (post 5*d.*)

Index to all Reports and Memoranda published in the Annual Technical Reports

1909–1947 R. & M. 2600 (out of print)

Indexes to the Reports and Memoranda of the Aeronautical Research Council

Between Nos. 2351–2449	R. & M. No. 2450	2*s.* (post 3*d.*)
Between Nos. 2451–2549	R. & M. No. 2550	2*s.* 6*d.* (post 3*d.*)
Between Nos. 2551–2649	R. & M. No. 2650	2*s.* 6*d.* (post 3*d.*)
Between Nos. 2651–2749	R. & M. No. 2750	2*s.* 6*d.* (post 3*d.*)
Between Nos. 2751–2849	R. & M. No. 2850	2*s.* 6*d.* (post 3*d.*)
Between Nos. 2851–2949	R. & M. No. 2950	3*s.* (post 3*d.*)
Between Nos. 2951–3049	R. & M. No. 3050	3*s.* 6*d.* (post 3*d.*)
Between Nos. 3051–3149	R. & M. No. 3150	3*s.* 6*d.* (post 3*d.*)

Printed and published by
HER MAJESTY'S STATIONERY OFFICE

To be purchased from
York House, Kingsway, London W.C.2
423 Oxford Street, London W.1
13A Castle Street, Edinburgh 2
109 St. Mary Street, Cardiff
39 King Street, Manchester 2
50 Fairfax Street, Bristol 1
35 Smallbrook, Ringway, Birmingham 5
80 Chichester Street, Belfast 1
or through any bookseller

Printed in England

R. & M. No. 3295

S.O. Code No. 23-3295